LAWRENCE
LIVERMORE
NATIONAL
LABORATORY

UCRL-JRNL-208832

Facile Synthesis of a Crystalline, High-Surface Area SnO2 Aerogel

T. F. Baumann, S. O. Kucheyev, A. E. Gash, J. H. Satcher, Jr.

January 4, 2005

Advanced Materials

Facile Synthesis of a Crystalline, High-Surface Area SnO_2 Aerogel

Theodore F. Baumann, S. O. Kucheyev, Alexander E. Gash, and Joe H. Satcher, Jr.*

Lawrence Livermore National Laboratory, Chemistry and Material Science Directorate, Livermore, California 94551

AUTHOR EMAIL ADDRESS: baumann2@llnl.gov

RECEIVED DATE ( )

KEYWORDS: Tin dioxide, sol-gel, monolith, epoxide, SnO_2

ABSTRACT: We report the preparation of a novel monolithic SnO_2 aerogel using a straightforward sol-gel technique. TEM and XRD analysis show that the as-prepared material is comprised of interconnected, randomly oriented crystalline (rutile) SnO_2 nanoparticles ~3–5 nm in size. As a result, the low-density SnO_2 monolith (~97% porous) exhibits a very high surface area of 383 m^2/g. XANES spectroscopy at the Sn $M_{4,5}$ edge reveals that the electronic structure of the SnO_2 aerogel is similar to that of tetragonal SnO rather than SnO_2 or □-Sn, and that the undercoordinated surface atoms in the material introduce additional Sn-related electronic states close to the conduction band minimum.

Table of Contents Graphic

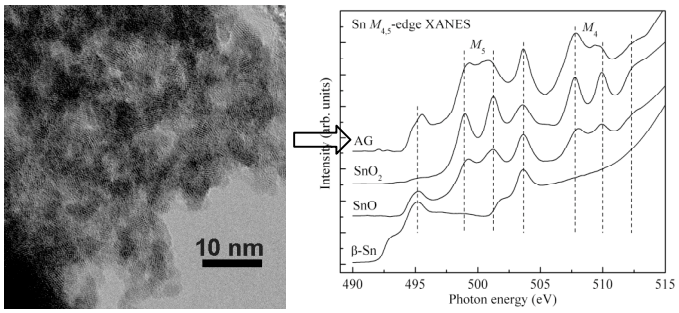

Introduction. Since the size, morphology, and dimensionality of semiconductors impact their properties, significant efforts have been dedicated to the design of nanostructured semiconductor materials to improve their performance in optical, electronic and electrochemical applications.[1] Tin dioxide (SnO_2) is a wide band gap semiconductor (with a room-temperature band gap of ~3.6 eV) that has been widely used in gas sensors,[2-6] optical devices,[7] and lithium batteries.[8-10] Previous studies have shown that the performance of SnO_2 materials in sensor and electrode applications is intimately tied to a number of important structural features, such as crystallite size, surface-to-volume ratio and surface electronic properties. For example, it has been demonstrated that the gas sensitivity of nanocrystalline SnO_2 sensors increases drastically as the size of SnO_2 crystallites decreases below ~10 nm.[2]

Several methods have recently been reported for the preparation of SnO_2 nanostructures, including sol-gel,[11-16] anodic oxidation,[17] physical/chemical vapor deposition,[18,19] thermal oxidation,[20] and microwave irradiation approaches.[21] Most of these previous efforts have focused on the synthesis of low-dimensional SnO_2 nanomaterials such as nanoparticles,[22-24] nanorods,[25,26] and nanobelts.[27] There are fewer examples in the literature of porous 3D SnO_2 nanostructures.[11-14,20] This is not surprising since the solution-based techniques used to prepare 3D SnO_2 nanostructures commonly require highly reactive tin precursors, complex solvent systems, and/or elevated temperatures.[11-16] In this letter, we describe the synthesis of a monolithic, high-surface area SnO_2 aerogel using a facile and straightforward sol-gel technique. Structural characterization shows that this novel material consists of an interconnected network of

crystalline (rutile) SnO_2 nanoparticles and, as a result, exhibits the open-cell porosity and high surface-to-volume ratio that are particularly important for sensor design.

Experimental Section. The reactants used in this preparation, $SnCl_4 \cdot 5H_2O$ and propylene oxide, were obtained from Aldrich. In a typical synthesis, $SnCl_4 \cdot 5H_2O$ (0.56 g, 1.6 mmol) was dissolved in 2.5 mL of water, followed by the addition of propylene oxide (1.02 g, 17 mmol) to the clear solution. The reaction mixture was stirred for 2 min, transferred to a plastic mold, and the solution was allowed to gel at room temperature for 24 h. Gel formation typically occurred within ~10 min, affording a translucent monolith. The monolithic gel was then soaked in a bath of absolute ethanol for 1 day to exchange the water and reaction by-products from the pores of the material. The wet tin oxide gel was processed in a Polaron™ critical point extractor. The ethanol in the pores of the wet gel was exchanged with liquid CO_2 for 3-4 days, after which time, the temperature was ramped up to ~45ºC, while maintaining a pressure of ~100 bars. The autoclave was then depressurized at a rate of ~ 7 bar/h, affording the material as a right circular cylinder (volume ~ 2.2 cm^3) with typical densities between 0.20–0.25 g/cm^3 (~97% porous solids). The bulk density of the aerogel was determined by measuring the dimensions and mass of the monolithic sample.

The microstructure of the tin oxide aerogel was studied by bright-field high-resolution transmission electron microscopy (HRTEM) performed in a Philips CM300FEG electron microscope operating at 300 keV. Powder x-ray diffraction (PXRD) data were collected using an APD3720 PEI diffractometer with a Cu K radiation source. Surface area determination and pore volume and size analysis were performed by Brunauer-Emmett-Teller (BET) and Barrett-Joyner-Halenda (BJH) methods using an ASAP 2000 Surface

Area Analyzer (Micromeritics Instrument Corporation). Samples of ~0.1 g were heated to 150 ºC under vacuum (10^{-5} Torr) for at least 24 hours to remove adsorbed species. Nitrogen adsorption data were then taken at five relative pressures from 0.05 to 0.20 at -196 ºC to calculate the surface area by BET theory.[28] For BJH analyses, average pore size and pore volume were calculated using data points from the desorption branch of the isotherm. Soft x-ray absorption near-edge structure (XANES) spectroscopy experiments were performed at undulator beamline 8.0 at the Advanced Light Source; Lawrence Berkeley National Laboratory.[29] Spectra were obtained by recording the total electron yield (TEY). After a linear background subtraction, all XANES spectra were normalized to the post-edge step heights.

Results and Discussion. The SnO_2 aerogel was prepared based on a general epoxide-initiated gelation method recently developed in our laboratory.[30,31] In this approach, the epoxide acts as an acid scavenger in the sol-gel polymerization reaction, driving the hydrolysis and condensation of the hydrated metal species. During the gelation process, the slow and uniform increase in the pH of the solution leads to the formation of hydrolyzed metal species, which link together through olation and oxolation to give a sol of metal oxide particles that subsequently cross-link to produce a monolithic gel. The epoxide is ultimately consumed in the gelation reaction generating ring-opened by-products. In this particular case, the hydrated Sn(IV) ion acts as the acid and, following the addition of propylene oxide, generates hydroxylated species that serve as the building blocks for the condensed phase. Following gelation, the wet SnO_2 gel monolith was dried using supercritical carbon dioxide extraction to preserve the open-cell architecture of the extended structure.

The morphology of the as-prepared SnO_2 aerogel was evaluated using HRTEM. As shown in Figure 1, the skeletal aerogel network is composed of interconnected spheroidal particles, ~3–5 nm in size. Examination of the higher magnification HRTEM micrograph, shown in Figure 2, reveals that these nanoparticles are highly crystalline, as evidenced by well-defined lattice fringes. The powder XRD analysis of the aerogel indicates that the SnO_2 nanoparticles have a rutile (cassiterite) structure (Figure 3). This is an important result since other solution-based techniques typically require elevated reaction temperatures or an additional post-preparation annealing step to induce particle recrystallization.[11-16] In addition, the XRD data reveal no evidence of the tetragonal (romarchite) SnO phase in the material. The textural porosity of the SnO_2 aerogel was investigated using nitrogen adsorption/desorption techniques. The material exhibited a high BET surface area of 383 m^2/g, an average BJH pore

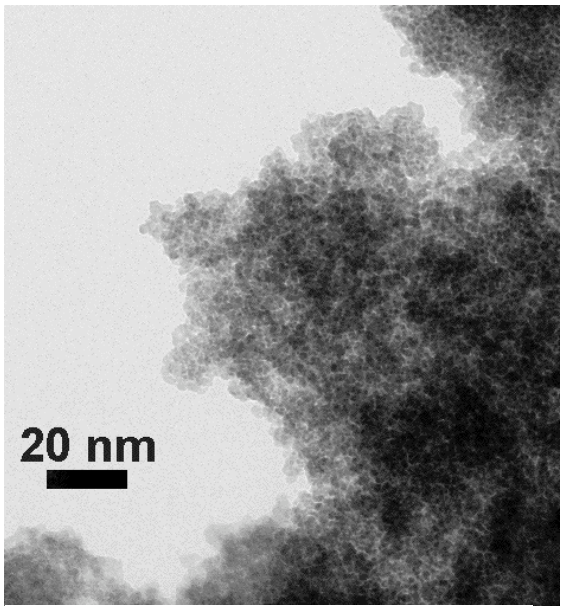

Figure 1. Bright field TEM image of the SnO_2 aerogel.

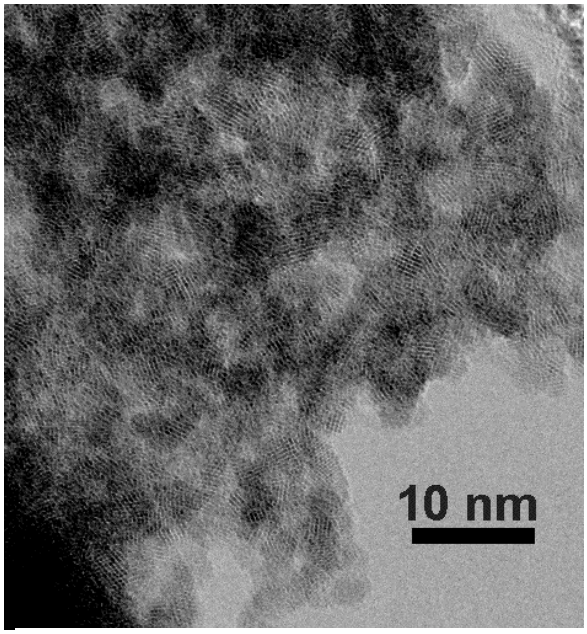

Figure 2. HRTEM image of the SnO_2 aerogel showing the lattice fringes of the crystalline nanoparticles.

diameter of 20 nm, and a pore volume of 2.3 ml/g. The adsorption/desorption isotherm was type IV with a H1 hysteresis loop, consistent with the network structure of spherical primary particles revealed in the HRTEM images.

Since gas sensor applications of SnO_2 are related to surface electronic properties, we examined the electronic structure of the SnO_2 aerogel using XANES spectroscopy. A comparison of the Sn $M_{4,5}$-edge XANES spectrum for the SnO_2 aerogel to those for full-density SnO_2, SnO, and β-Sn reference samples is given in Figure 4. Such Sn $M_{4,5}$-edge spectra reflect electron transitions from the Sn 3*d* core level (spin-orbit split into $3d_{3/2}$ and $3d_{5/2}$ levels, giving rise to M_4 and M_5 edges, respectively) into unoccupied electronic states above the Fermi level. If core-hole and electron correlation effects are ignored, such spectra essentially map Sn-related *p*- and *f*-projected states in the conduction band. Our detailed study of the electronic structure of SnO_2 nanostructures, with the symmetry assignment of XANES peaks, is beyond the scope of this letter and will be reported separately.[32] Nevertheless, it is

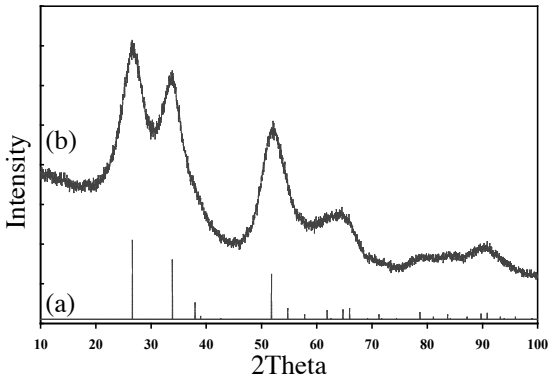

Figure 3. (a) Expected peak positions and relative intensities for cassiterite (rutile) SnO_2 (JCPDS no. 41-1445) and (b) the powder XRD pattern for the SnO_2 aerogel.

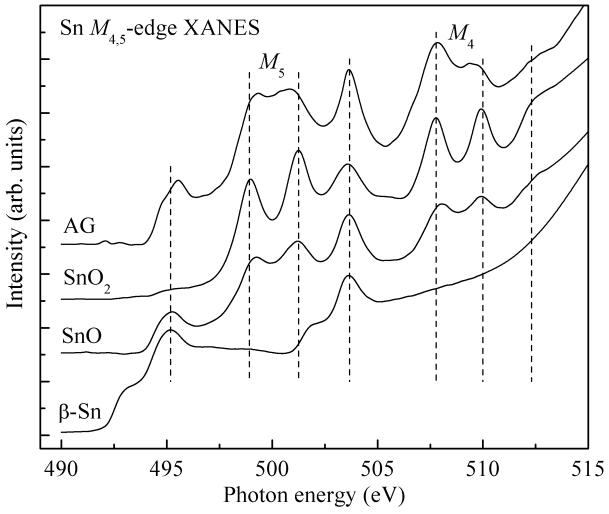

Figure 4. Tin $M_{4,5}$-edge XANES spectrum of the SnO_2 aerogel (labeled AG) compared with spectra from full-density SnO_2, tetragonal SnO, and β-Sn reference samples.

important to note that the surface electronic structure of the as-prepared SnO_2 aerogel is more similar to that of full-density SnO rather than SnO_2 or □-Sn. The data in Figure 4 also show that under-coordinated surface atoms in the SnO_2 aerogel introduce additional Sn-related electronic states close to the conduction band minimum (~494 eV in Figure 4).[32] This finding is somewhat surprising since our XRD analysis has revealed no evidence of the tetragonal SnO phase in the nanostructure. These XANES results, however, are consistent with previous observations by valence-band x-ray photoelectron spectroscopy that the surface electronic structure of full-density (bulk) SnO_2 often resembles that of SnO.[33] Due to the large surface-to-volume atom fraction in our material, this apparent oxygen deficiency is revealed even with a technique (TEY XANES) that probes the entire volume of the nanoligaments comprising the skeletal aerogel structure.

Conclusion. In summary, we have reported the preparation and properties of a novel monolithic SnO_2 aerogel using a facile sol-gel technique. Microstructural analysis has shown that the as-prepared material (without any post-preparation annealing steps) consists of a continuous network of interconnected crystalline (rutile) SnO_2 nanoparticles. As a result, the low-density SnO_2 aerogel possesses high surface area and continuous porosity. The synthetic flexibility of the epoxide-initiated gelation process presents the opportunity for future systematic studies of SnO_2 nanoarchitectures with the goal of optimizing material properties for specific applications. For example, we have shown that the structural properties (e.g. crystallite size and shape, surface area, and porosity) of metal oxide aerogels prepared by this method can be modified by simply changing a single synthetic parameter in the sol-gel reaction, such as the type of epoxide or the anion

of the metal salt.[34,35] In addition, this facile sol-gel method is amenable to the preparation of mixed metal-oxide systems,[36] providing access to novel doped-SnO_2 nanomaterials.

Acknowledgements. Special thanks are to J. Harper for HRTEM analysis and C. Saw for XRD data. Work was performed under the auspices of the U.S. DOE by Univ. of CA, Lawrence Livermore National Laboratory under contract number W-7405-ENG-48. The ALS is supported by the Director, Office of Science, Office of BES, Materials Sciences Division, of the U.S. DOE under Contract No. DE-AC03-76SF00098 at LBNL.

References

1. Ng, H. T.; Li, J.; Smith, M. K.; Nguyen, P.; Cassell, A.; Han, J.; Meyyappan, M. *Science* **2003**, *300*, 1249.

2. Shukla, S.; Seal, S.; Ludwig, L.; Parish, C. *Sens. Actuators B* **2004**, *97*, 256.

3. Sahm, T.; Mädler, L.; Gurlo, A.; Barsan, N.; Pratsinis, S. E.; Weimar, U. *Sens. Actuators B* **2004**, *98*, 148.

4. Shukla, S.; Patil, S.; Kuiry, S. C.; Rahman, Z.; Du, T.; Ludwig, L.; Parish, C.; Seal, S. *Sens. Actuators B* **2003**, *96*, 343.

5. Salehi, A. *Sens. Actuators B* **2003**, *96*, 88.

6. Torkhov, D. S.; Burukhin, A. A.; Churagulov, B. R.; Rumyantseva, M. N.; Maksimov, V. D. *Inorg. Mater.* **2003**, *39*, 1158.

7. Ginley, D. S.; Bright, C. *MRS Bulletin* **2000**, *25*, 15.

8. Huang, F.; Yuan, Z.; Zhan, H.; Zhou, Y.; Sun, J. *Mater. Lett.* **2003**, *57*, 3341.

9. Retoux, R.; Brousse, T.; Schleich, D. M. *J. Electrochem. Soc.* **1997**, *146*, 2472.

10. Idota, Y.; Kubota, T.; Matsufuji, A.; Maekawa, Y.; Miyasaka, T. *Science* **1997**, *276*, 1395.

11. Huang, R.; Hou, L.; Zhou, B.; Zhao, Q.; Ren, S. *J. Non-Cryst. Solids* **2005**, *351*, 23.

12. Harreld, J. H.; Sakamoto, J.; Dunn, B. *J. Power Sources* **2003**, *115*, 19.

13. Briois, V.; Santilli, C. V.; Pulcinelli, S. H.; Brito, G. E. S. *J. Non-Cryst. Solids* **1995**, *191*, 17.

14. Tung, C. Y.; Wu, N. L.; Rusakova, I. A. *J. Mater. Res.* **2003**, *18*, 2890.

15. Briois, V.; Belin, S.; Zucolotto Chalaça, M.; Santos, R. H. A.; Santilli, C. V.; Pulcinelli, S. H. *Chem. Mater.* **2004**, *16*, 3885.

16. Toupance, T.; Babot, O.; Jousseaume, B.; Vilaça, G. *Chem. Mater.* **2003**, *15*, 4691.

17. Shin, H. C.; Dong, J.; Liu, M. *Adv. Mater.* **2004**, *16*, 237.

18. Wang, Z. L. *Ann. Rev. Phys. Chem.* **2004**, *55*, 159.

19. Deng, H.; Lamelas, F. J.; Hossenlopp, J. M. *Chem. Mater.* **2003**, *15*, 2429.

20. Chen, A.; Peng, X.; Koczkur, K.; Miller, B. *Chem. Commun.* **2004**, 1964.

21. Zhu, J. J.; Zhu, J. M.; Liao, X. H.; Fang, J. L.; Zhou, M. G.; Chen, H. Y. *Mater. Lett.* **2002**, *53*, 12.

22. Leite, E. R.; Maciel, A. P.; Weber, I. T.; Lisboa-Filho, P. N.; Longo, E.; Paiva-Santos, C. O.; Andrade, A. V. C.; Pakoscimas, C. A.; Maniette, Y.; Schreiner, W. H. *Adv. Mater.* **2002**, *14*, 905.

23. Pang, G.; Chen, S.; Koltypin, Y.; Zaban, A.; Feng, S.; Gedanken, A. *Nano Lett.* **2001**, *1*, 723.

24. Wu, N. L.; Wang, S. Y.; Rusakova, I. A. *Science* **1999**, *285*, 1375.

25. Liu, Y.; Dong, J.; Liu, M. *Adv. Mater.* **2004**, *16*, 353.

26. Zhang, D. F.; Sun, L. D.; Yin, J. L.; Yan, C. H. *Adv. Mater.* **2003**, *15*, 1022.

27. Comini, E.; Guidi, V.; Malagù, C.; Martinelli, G.; Pan, Z.; Sberveglieri, G.; Wang, Z. L. *J. Phys. Chem. B* **2004**, *108*, 1882.

28. Gregg,S. J.; Sing, K. S. W. *Adsorption, Surface Area and Porosity*, 2nd ed., Academic Press, London, 1982.

29. Jia, J. J.; Callcott, T. A.; Yurkas, J.; Ellis, A. W.; Himpsel, F. J.; Samant, M. G.; Stohr, J.; Ederer, D. L.; Carlisle, J. A.; Hudson, E. A.; Terminello, L. J.; Shuh, D. K.; Perera, R. C. C. *Rev. Sci. Instrum.* **1995**, *66*, 1394.

30. Baumann, T. F.; Gash, A. E.; Fox, G. A.; Satcher, J. H.; Hrubesh, L. W. In *Handbook of Porous Solids*; Schuth, F., Sing, K. S., Weitkamp, J., Eds.; Wiley-VCH: Weinheim, 2002; Vol. 3, p 2014.

31. Gash, A. E.; Tillotson, T. M.; Satcher, J. H.; Poco, J. F.; Hrubesh, L. W.; Simpson, R. L. *Chem. Mater.* **2001**, *13*, 999.

32. Kucheyev, S. O.; Baumann, T. F.; van Buuren, T; Wang, Y. M.; Satcher, J. H.; Hamza, A. V. *manuscript in preparation.*

33. Sanjines, R; Coluzza, C.; Rosenfeld, D.; Gozzo, F.; Almeras, Ph.; Levy, F.; and Margaritondo, G. *J. Appl. Phys.* **1993**, *73*, 3997.

34. Gash, A. E.; Satcher, J. H.; Simpson, R. L. *Chem. Mater.* **2003**, *15*, 3268.

35. Baumann, T. F.; Gash, A. E.; Chinn, S. C.; Sawvel, A. M.; Maxwell, R. S.; Satcher, J. H. *Chem. Mater.* **2005**, *in press.*

36. Clapsaddle, B. J.; Gash, A. E.; Satcher, J. H.; Simpson, R. L. *J. Non-Cryst. Solids* **2003**, *331*, 190.